EUROPEAN FUSION DEVELOPMENT AGREEMENT

EFDA–JET–PR(04)76

V.V. Plyusnin, V. Riccardo, R. Jaspers, B. Alper, V.G. Kiptily, J. Mlynar,
S. Popovichev, E. de La Luna, F. Andersson, and JET-EFDA contributors

Study of Runaway Electron Generation During Major Disruptions in JET.

Study of Runaway Electron Generation During Major Disruptions in JET.

V.V. Plyusnin[1], V. Riccardo[2], R. Jaspers[3], B. Alper[2], V.G. Kiptily[2], J. Mlynar[4], S. Popovichev[2], E. de La Luna[5], F. Andersson[6], and JET-EFDA contributors*

[1]Association Euratom-IST, Centro de Fusão Nuclear, Lisbon, Portugal
[2]Euratom /UKAEA Fusion Association, Culham Science Centre, Abingdon, UK
[3]Association Euratom-FOM, Nieuwegein, The Netherlands
[4]Association Euratom - IPP.CR, Prague, Czech Republic
[5]Association Euratom-CIEMAT, Madrid, Spain
[6] VR-Euratom Association, Chalmers University of Technology, Gothenburg, Sweden
**See appendix of J. Pamela et al., Fusion Energy 2004*
(Proc. 20th IAEA Conference, Vilamoura, portugal 2004

Preprint of Paper to be submitted for publication in
Nuclear Fusion

ABSTRACT

Extensive analysis of disruptions in JET has enabled an advance in the understanding of disruption generated runaway electrons. Tomographic reconstruction of the soft X-ray emission has made possible a detailed observation of the magnetic flux geometry evolution during disruptions. With the aid of soft and hard X-ray diagnostics the runaway electrons have been detected at the very beginning of disruptions. A study of runaway electron parameters has shown that an approximate upper bound for the conversion efficiency of pre-disruptive plasma currents into runaways is about 60% over a wide range of the plasma currents in JET. Runaway generation has been simulated with a test particle model in order to verify the results of experimental data analysis and to obtain the background for extrapolation of the existing results onto larger devices like ITER. It was found that close agreement between the modelling results and experimental data could be achieved if in the calculations the post-disruption plasma electron temperature was assumed equal to 10eV and if the plasma column geometry evolution is taken into account in calculations. The experimental trends and numerical simulations show that runaway electrons are a critical issue for ITER and, therefore, the development of mitigation methods, which suppress runaway generation, is an essential task.

1. INTRODUCTION.

Runaway Electrons (REs) with energies in the range from several MeV till to several tens of MeV have been observed during numerous disruptions in large tokamaks, such as JET [1-3], JT-60U [4, 5], TFTR [6], TORE SUPRA [7]. The interaction of RE beams with Plasma Facing Components (PFC) resulted in large heat loads, melting and sputtering of the armour material and of the vacuum chamber itself. In future reactor-scale devices, like ITER [8], localized deposition of several Mega-Amperes of multi-MeV RE currents onto the first wall will inevitably cause its severe damage. In order to elaborate efficient methods to minimize the deleterious effects of REs on PFC, a good understanding of the mechanisms responsible for RE generation and confinement is required both from a theoretical and an experimental point of view.

The experimental data on disruptions and disruption-generated REs has been collected since the beginning of JET operations [9]. In many disruptions a very high electron density ($n_e > 10^{20}$ m^{-3}), strong MHD activity or slow current quenches and electron temperatures of about $T_e \sim 100$eV after the thermal quench [2, 9, 10] were the reasons for absence of noticeable RE generation. However, a significant number of disruptions revealed intense RE generation.

In this paper we present recent results of RE studies in JET, which have been focused mainly on the disruptions with post-disruption current plateaux created by REs (I_{RE}). Prior to divertor installation the disruptions with plasma current (I_p) up to 6MA resulted in creation of long-lived RE plateaux ($t_{plateau} \sim 1$ sec) with I_{RE} up to 2-2.5MA. Divertor installation resulted in increased vertical instability of the current-carrying channel, thus substantially decreasing the duration of measured RE plateaux ($t_{plateau} \leq 100$ms). Despite this the RE plateaux with I_{RE} up to 1MA have been observed in various magnetic configurations with different toroidal magnetic fields and plasma

currents. Primary (Dreicer) acceleration [11] and secondary avalanching [12-14] are two mechanisms responsible for the creation of REs during disruptions. Both mechanisms have been simulated using a test particle model in order to reproduce experimental data and to obtain the background for extrapolation of the existing results onto larger devices, like ITER. It was found that close agreement between the modelling results and experimental data could be achieved if the plasma column geometry evolution is taken into account in calculations.

The results of numerical simulations and experimental data analysis show that disruption generated REs are a critical issue for ITER. Thus, the development of techniques, which suppress or mitigate RE generation, is essential in view of ITER operations. Some results on the development of these techniques in JET are discussed in this paper.

2. CHARACTERISTICS OF DISRUPTION GENERATED RUNAWAY ELECTRONS.

Spontaneous disruptions in JET provided extended data on REs generated at the different toroidal magnetic fields, plasma currents, triangularity and elongations. Intentional disruptions for RE studies have been produced by programmed noble gas puff (neon, argon or helium) in low elongation limiter configuration to ensure more stable behaviour of the RE beam during and after disruptions. An example of a long-lived RE beam generated at an intentional disruption provoked by neon puff (Pulse No: 63117, $I_{RE} \sim 1$MA, $t_{plateau} \sim 100$ms) is presented in Fig.1. The highest ratio of the generated RE current to pre-disruption plasma current (Pulse No: 53790, $I_{RE}/I_p \cong 0.6$, argon) is shown in Fig.2. RE beams interacting with cold post-disruption plasma produces detectable soft X-ray radiation ($E_\gamma << 1$MeV) [2]. The contour plots of the soft X-ray emission measured by the horizontal set of detectors [15] (Figs.1 and 2) provided the information on evolution of RE current-carrying channel in time and space. In the following, this data has been used in numerical modelling of the runaway process. The sequence of events in disruptions is well known and its detailed phenomenological description can be found elsewhere [1-6]. Large resistive electric fields occur at the thermal quench and cause the primary RE generation. Gaining very high energies the primary REs [2,16] inevitably will serve as a seed population for the secondary avalanche process [2, 11-13]. The interaction between these two mechanisms has been studied with the aid of numerical modelling carried out using a test particle model [17]. A set of equations (1)-(3) has been solved with initial conditions inferred from the experimental data (plasma current, density, etc.) or reasonably assumed plasma parameters (temperature, Z_{eff}, etc) [18].

$$\frac{dP_{\|}}{dt} = \frac{e}{m_e c} E_{\|} - \frac{e^4 n_e \ln\Lambda}{4\pi\varepsilon_0^2 m_e^2 c^3} \gamma(\gamma+\alpha) \frac{P_{\|}}{P^3} - \frac{e^4 n_e \ln\Lambda}{4\pi\varepsilon_0 m_e c^3} \frac{2B_0\varepsilon_0}{3 m_e n_e \ln\Lambda} \left(\frac{m_e^2 c^2}{e^2 B_0^2 R_0^2} + \frac{P_\perp^2}{P^4}\right) \gamma^4 \beta^3 \frac{P_{\|}}{P} \quad (1)$$

$$\frac{dP}{dt} = \frac{e}{m_e c} E_{\|} \frac{P_{\|}}{P} - \frac{e^4 n_e \ln\Lambda}{4\pi\varepsilon_0^2 m_e^2 c^3} \frac{\gamma^2}{P} - \frac{e^4 n_e \ln\Lambda}{4\pi\varepsilon_0^2 m_e^2 c^3} \frac{2B_0\varepsilon_0}{3 m_e n_e \ln\Lambda} \left(\frac{m_e^2 c^2}{e^2 B_0^2 R_0^2} + \frac{P_\perp^2}{P^4}\right) \gamma^4 \beta^3 \quad (2)$$

$$\frac{dn_{RE}}{dt} = \lambda_R \frac{n_{RE}}{\tau_{RE}} - \frac{n_{RE}}{t_0} \quad (3)$$

Where $\alpha = Z_{eff}+1$, $\lambda_R = C(Z_{eff}) n_e v_e \varepsilon^{-3(Zeff+1)/16} \exp\left[-\frac{1}{4\varepsilon} - \sqrt{\frac{(Z_{eff}+1)}{\varepsilon}}\right]$ – is the primary runaway generation rate, where $C(Z_{eff})$ is numerical coefficient: $C(Z_{eff}) \cong 0.4$ for $Z_{eff} = 4$ used in calculations,

$E_{||}(t) = -\frac{L_p}{2\pi R_0}\frac{dI_p(t)}{dt} = \eta_p j_p(t)\left(1\frac{-I_{RE}(t)}{I_p(t)}\right)$ – is the evolution of the parallel electric field,

$t_0 = \frac{4\pi\varepsilon_0 m_e c^3}{e^4 n_e}\sqrt{\frac{3}{\pi}(Z_{eff}+5)}\left(\frac{E_{||}}{E_{CR}} - 1\right)^{-1}$ – is the secondary avalanching growth characteristic time,

$P_{||}$, $P_{\perp}$, P – are the parallel, perpendicular and total electron momenta normalized to $m_e c$,
$P^2 = \gamma^2 - 1$,
γ – is the relativistic factor,
B_0 – is the toroidal magnetic field,
R_0 – is the plasma major radius,
n_{RE} – is the density of runaway electrons,
$E_{DR} = e^3 \ln\Lambda n_e Z_{eff}/4\pi\varepsilon_0{}^2 T_e$ – is the Dreicer field,
$E_{CR} = E_{DR}(T_e/m_e c^2)$,
$\varepsilon = E_{||}/E_{DR}$.

The dynamics of REs, which experience acceleration in the electric field (the first term on the right-hand side of Eqs.(1)-(2)), collisions with the plasma particles (the second term) and the sum of synchrotron radiation losses due to guiding centre motion and electron gyro-motion (the third term), has been simulated. Inclusion of the avalanching term into the equation for the RE density evolution (Eq.(3)) made it possible to clarify the role of the avalanching process at the early stage of disruption. The evolution of electric field in the plasma has been modelled taking into account that RE current substitutes the plasma resistive current and the plasma current decays exponentially during disruption with characteristic e-folding time $\tau_p = I_p*(dI_p/dt)^{-1} \equiv L_p/R_p$ inferred form the experimental data. For simplicity, it was assumed that REs are perfectly confined ($\tau_{RE} \to \infty$). Modelling provided close agreement between evolutions of the measured plasma current in disruption Pulse No: 63117 and total calculated current, which consists of two fractions: RE current (I_{RE}) and exponentially decaying plasma current (Fig.3(a)). Numerical simulations also show that the secondary avalanching process causes the most of the disruption generated REs (Fig.3(b)). Depending on the initial conditions the RE current densities being inferred from calculated n_{RE} can achieve values up to $j_{RE} = 1 MA/m^2$ with the maximal energy of relativistic electrons determined from calculated γ. Results of these simplified simulations agree well with detailed numerical modelling performed either by Monte Carlo simulation of the drift kinetic equation for relativistic electrons in toroidal geometry using the ARENA code or by solving a nonlinear system of equations for the runaway density that exploits earlier, analytical results on runaway production [19, 20].

Usually REs are detected when they produce the hard X-rays ($E_\gamma \geq 1$MeV) and photo-neutron emission ($E_\gamma >> 1$MeV). Quasi-stationary plateaux and intense bursts of hard X-ray emission show that an appreciable number of REs have energy well above 1MeV. The neutron emission rate has been determined using three ^{235}U fission chambers [21]. Photo-neutron emission observed during disruptions is the direct evidence that RE energies can be as high as 11MeV, if neutrons are caused by Fe(γ,n)-reaction, or even higher than 19MeV, if they are the result of ^{12}C(γ,n)-reaction. Using these threshold values the properties of REs have been examined in experimental data analysis and numerical modelling. In particular, two RE populations have been distinguished in disruptions: small population of very energetic REs and large RE fraction with relatively low energy. According to numerous studies [2-4,12-14] the distribution function of the primary REs is expected to be close to mono-energetic with very high average kinetic energy, while the secondary avalanche mechanism results in the nearly exponential RE distribution function at substantially lower energy. Large RE population created in Pulse No: 53790 resulted in a fast decay of the electric field due to current substitution effect. The efficiency of the Dreicer mechanism is decreased, but REs are still created due to secondary avalanching mechanism, which provide the lower energy of REs. The photo-neutron emission during Pulse No: 53790 (Fig.2) is still negligibly small at the large RE plateau and intense hard X-rays radiation. High bursts of the photo-neutron emission ($\geq 4\cdot10^{14}$ counts/s) have been observed only when some current filaments obviously containing high-energy REs (W_{RE}>10MeV) interacted with PFC. Unlike Pulse No: 53790, steady-state photo-neutron emission ($\sim2\cdot10^{14}$ counts/s) in Pulse No: 63117 indicated that substantially larger fraction of high-energy REs is present during smaller current plateau. Thus, the larger population of high energy REs is caused by less current substitution effect. These two experimental cases have been analysed using numerical simulations. The evolution of the test runaway electron in a momentum space and temporal evolution of RE density have been modelled assuming that the cross-section of RE beam might have different size during current quench phase. Calculated trajectories of accelerated test electron in momentum space and evolution of RE density for two cross-sections of RE beam ($a_{beam2} = 2a_{beam1}$) are presented in Figs.4(a) and 4(b). Increase of RE current (as a result of larger beam cross-section) at other equal initial plasma and runaway generation parameters decreases the maximal RE densities and energies. Note, that close correspondence of the modelled and measured currents in Fig.3(a) has been obtained with taking into account the evolution of the beam cross-section.

3. EVOLUTION OF MAGNETIC CONFIGURATION DURING DISRUPTIONS.

Modelling of runaway process during the thermal quenches [16, 22] shows that due to the continuous character of the electron acceleration, significant RE populations should already exist at the beginning of current quench stage. On the other hand, REs are sensitive to magnetic fluctuations, which decrease the characteristic life-time of the runaways: $\tau_{RE}=a^2/5.8D_r$, where $D_r \approx \pi q R_0 c(b_r/B_0)^2$ is the coefficient of the radial diffusion caused by the presence of magnetic field perturbations with the magnitude b_r. Very large magnetic perturbations lead to the enhanced losses of fast particles and limit the energy and total amount of REs [2]. Hard X-ray bursts during the negative loop voltage

spikes show that substantial populations of REs with energies in the MeV-energy range have been created in the early stages of a disruption and survived to the current quench phase. The strong dependence of the runaway process on the magnetic turbulence level makes impossible the prediction of the RE parameters evolution within the frame of a test particle model. To simulate the evolution of the RE parameters at this stage of disruptions it is necessary to take into account the strong influence of the magnetic configuration evolution on REs confinement, which constitutes a separate very complicated task [23].

The soft X-ray measurements, despite their qualitative character, have provided important information about the evolution of the magnetic field structure during disruptions [24,25]. Tomographic reconstruction of the soft X-ray emission [26] in the immediate proximity and during the negative voltage spikes allowed observation of strong re-arrangement of the magnetic configuration. This analysis has been performed taking into account that the energy isotropisation along the magnetic field lines is still considerably faster than the evolution of the MHD modes [24,25,27,28]. Therefore, the assumption that the soft X-ray emission is constant on a magnetic flux surface remains valid throughout this stage. The soft X-ray diagnostics [14], used here, consists of two soft X-ray cameras, one vertical and one horizontal. The vertical pinhole camera is located at the top of the vessel with a multi-channel photodiode array that provides 35 viewing lines. The horizontal camera is located at the low field side and has 17 separate photodiode channels. Beryllium foil windows and depth of photodiode sensitive layer enabled the detection of the soft X-ray emission in the energy range 2 keV $\leq E_\gamma \leq$ 10keV. A constrained optimization method on a rectangular grid with a distance between the grid points of 7.5cm was applied [26]. The set of equations relating soft X-ray emissivity in grid points to detected line integrals is heavily underdetermined, besides tomographic inversion being ill-conditioned by nature. The main constraint for physically acceptable solutions is the smoothness of the reconstructed emission image. In the JET tomographic inversion algorithm, the smoothness of soft X-ray emission is expected to be an order of magnitude higher along flux surfaces than along the plasma profile. The smoothing level is then set in an iterative process so that the reconstructed soft X-ray emission provides line integrals that fit best within the given data error-bars.

Figure 5 presents the evolution of the magnetic configuration in disruption Pulse No: 53790 as a sequence of soft X-ray tomographic images. They provide a detailed view of the disruption reconnection event with expulsion of the plasma core and subsequent formation of nested magnetic surfaces in the plasma core on a time scale of hundreds of microseconds. Therefore, initial confining conditions for existing population of super-thermal or low energy runaway electrons are created very soon after magnetic flux reconnections. As the runaway electrons gain more energy at the current quench, the soft X-ray bursts become a consequence of the interaction of the runaway beam with heavy impurity atoms [2] when it hits the surrounding surfaces of the device. A clear coincidence between the bursts of hard X-rays and neutron emissions and the appearance of the soft X-rays bursts when the runaway beam hits the wall has been observed.

4. EXPERIMENTAL SUMMARY AND DISCUSSION ON THE METHODS FOR AVOIDANCE OF RUNAWAY ELECTRONS.

In this chapter we summarize the experimental data obtained before and after divertor installation and analyse the trends of disruption-generated REs. A fairly linear dependence of the RE current plateaux on plasma current derivatives and pre-disruptive plasma currents allows the establishment of an approximate upper bound for the conversion efficiency of pre-disruptive plasma currents into runaways of about 60% over a wide range of the plasma currents in JET (Fig.6(a,b)). Plasma current decay times or JET disruptions are concentrated in a range between 10ms and 20ms over a wide variation of the pre-disruption plasma currents. Analysis of this data yields the values of post-disruption electron temperature T_e = 10-15eV at given plasma inductance $L_p = 4.5 \cdot 10^{-6}$ H [2]. With these T_e values the numerical modelling predicts a RE current conversion rate similar to that observed in experiments. Detailed numerical simulations [19,20] show that the current conversion efficiency in ITER could reach 60% leading to the generation of RE currents of about 10 MA with significantly better confinement of runaways. The RE plateaux current observed in JET has a non-linear dependence on B_0 (Fig.7) above a certain threshold in toroidal magnetic field ($B_0 \tilde{=} 2$ T) [2,3]. In fact, a doubling of the toroidal magnetic field resulted in an increase of the photo-neutron production by two orders of magnitude [3].

Summary trends of the data on REs observed at disruptions prior and after divertor installation and the results of numerical modelling suggest that in disruptions, which might occur at the ITER nominal Q=10 parameters ([29]: I_p=15 MA, $n_e = 10^{20}$ m^{-3}, MHD safety factor q_{95} =3) the generated runaway current could reach 10MA in the MeV energy range. Such intense RE beams inevitably will damage the device. To avoid these deleterious effects, the methods for RE suppression using intense puff of noble gases and auxiliary RF plasma heating have been studied. Different noble gases used for disruption initiations have different effects on the evolution of the disruption as well as on the RE generation. Disruptions provoked by puffs of argon or neon usually lead to a very fast thermal quench and often to intense RE generation. Unlike argon and neon, the use of helium has shown the absence of REs [30] due to very fast increase of the plasma density and smaller plasma current derivatives. However, longer current quench stage leads to large electromagnetic forces. Therefore, it remains essential to search the effective procedures to simultaneously suppress RE generation, mitigate large electromagnetic forces and heat loads during disruptions. Another approach to avoid RE generation during disruptions is to use auxiliary plasma heating to decrease high resistive electric fields and plasma current derivatives. In the general case, additional plasma heating can be used for amelioration of disruptions, when degradation of plasma parameters will be compensated by additional radio-frequency plasma heating. Electron Cyclotron Heating (ECH) in T-10 experiments [24] has demonstrated very promising results on the possibility to avoid (ameliorate) or to postpone disruption events. FTU experiments [31] having the purpose to suppress RE generation using ECH also revealed the possibility to ameliorate the disruptions themselves. Several pulses in JET have been carried out with the purpose to suppress RE generation using Low Hybrid Waves. However, these attempts did not reveal any effect due to poor coupling and low heating power density in the plasma core in JET.

CONCLUSIONS

1. Soft X-ray emission tomography has allowed the observation of the magnetic configuration evolution during a disruption. After fast expulsion of the hot plasma core, subsequent formation of confining magnetic structures and creation of a narrow current carrying channel has been observed. Such a configuration provided the confinement of existing runaway electrons.

2. A significant amount of primary REs with energies up to 2 MeV can be generated in the early stages of a JET disruption. These energetic electrons are observed when the strong magnetic perturbations cause the release of REs onto the plasma facing components in JET and hence the appearance of hard X-rays.

3. Two populations of runaway electrons have been found during runaway current plateaux. Small high-energy RE population have existed for a long time providing the creation of the secondary runaway electrons with significantly lower energy. Release of high-energy RE population onto walls resulted in appearance of intense neutron emission (up to 10^{16} counts per second).

4. With the increase of sizes, magnetic field and currents in tokamak experiments the disruption generated runaway currents might be up to 60% of the pre-disruptive currents. At ITER nominal parameters the estimated runaway currents can reach 10MA in the MeV-energy range. At these parameters runaway electrons will inevitably cause severe damage of the device if they are locally deposited onto the components of the first wall. JET experiments have shown that avoiding of runaway electron generation during disruptions can be achieved with the use of massive helium puff.

ACKNOWLEDGEMENTS

This work has been carried out within the framework of the Contract of Association between the European Atomic Energy Community and "Instituto Superior Técnico". Financial support was also received from "Fundação para a Ciência e Tecnologia" and""Programa Operacional Ciência, Tecnologia, Inovação do Quadro Comunitário de Apoio III".

The authors express sincere gratitude to Per Helander for his valuable support and helpful discussions.

REFERENCES

[1]. J. Wesson, R.D. Gill, M. Hugon et al. Nuclear Fusion **29** (1989) 641
[2]. R.D. Gill et al. Nuclear Fusion **42** (2002)1039
[3]. V. Riccardo, Plasma Phys. Contr. Fusion, **45** (2003) A269 -A284
[4]. R. Yoshino, S. Tokuda. Nuclear Fusion **40** (2000) 1293
[5]. Y. Kawano et al. Fusion Science and Technology **42** (2002) 298-314
[6]. E.D. Fredricson et al. Physics of Plasmas **4** (1997) 1589-1595

[7]. G. Martin. Proc. of the 1998 ICPP & 25th EPS Conf. on Plasma Physics and Controlled Fusion, Prague, Czech Republic, 1998, ECA, Vol **22C**, Report P3-006
[8]. ITER Physics Basis, Nuclear Fusion **39** (1999) 2137-2638
[9]. G.R. Harris. Comparison of the current decay during carbon-bounded and beryllium-bounded disruptions in JET. JET-R(90)07. JET preprint. 1990
[10]. V.V. Plyusnin et al. Proc. of the 30th EPS Conf. on Controlled Fusion & Plasma Physics, St. Petersburg, Russia, 2003, 7-11 July, ECA, Vol **27A** Report P2.94
[11]. H. Dreicer. Physical Review 115 (1959) 238
[12]. Yu.A. Sokolov. JETP Letters 29 (1979) 218
[13]. M.N. Rosenbluth and S. V. Putvinski. Nuclear Fusion **37** (1997) 1355
[14]. N.T. Besedin, I.M. Pankratov, Nuclear Fusion **26** (1986) 807.
[15]. B. Alper et al. Rev. Sci. Instrum. 68(1) (1997) 778
[16]. V.V. Plyusnin et al. Plasma Phys. Contr. Fusion **44** (2002) 2021–2031
[17]. B. Esposito et al. Physics of Plasmas **6** (1999) 238-252
[18]. D.G. White et al. Physics of Plasmas, **7** (2000) 4052
[19]. P. Helander et al. Plasma Phys. Control. Fusion **44** (2002) B247–B262
[20]. L.-G. Eriksson, P. Helander, F. Andersson, D. Anderson, and M. Lisak. Phys. Review Lett. 92 (2004) 205004
[21]. O.N. Jarvis. Treatment of the KN1 data channels. JET-TN(87)04. JET preprint. 1987
[22]. P. Helander et al. Physics of Plasmas, **11** (2004) 5704
[23]. P. Helander, L.-G. Eriksson, F. Andersson. Physics of Plasmas **7**(2000) 4106-4111
[24]. P.V. Savrukhin, E.S. Lyadina, D.A. Martynov, D.A. Kislov, V.I. Poznyak. Nuclear Fusion **34**
[25]. J. Howard, M. Persson. Nuclear Fusion 32(1992)361
[26]. L.C. Ingesson et al. Nuclear Fusion 38 (1998) 1675
[27]. S.V. Mirnov et al. Physics of Plasmas, 5 (1998) 3950
[28]. F.C. Shuller. Plasma Phys. Contr. Fusion 37 (1995) A135–A162–
[29]. R. Aymar et al. Nuclear Fusion 41 (2001) 1301
[30]. V. Riccardo et al., Plasma Phys. Contr. Fusion, 45 (2002) 905
[31]. B.Angelini, S.V. Annibaldi, C. Gormezano et al. Overview of the FTU results. Proceedings of the 20th IAEA Fusion Energy Conference, Vilamoura, Portugal, 2004, Report CN/116-OV/4-6

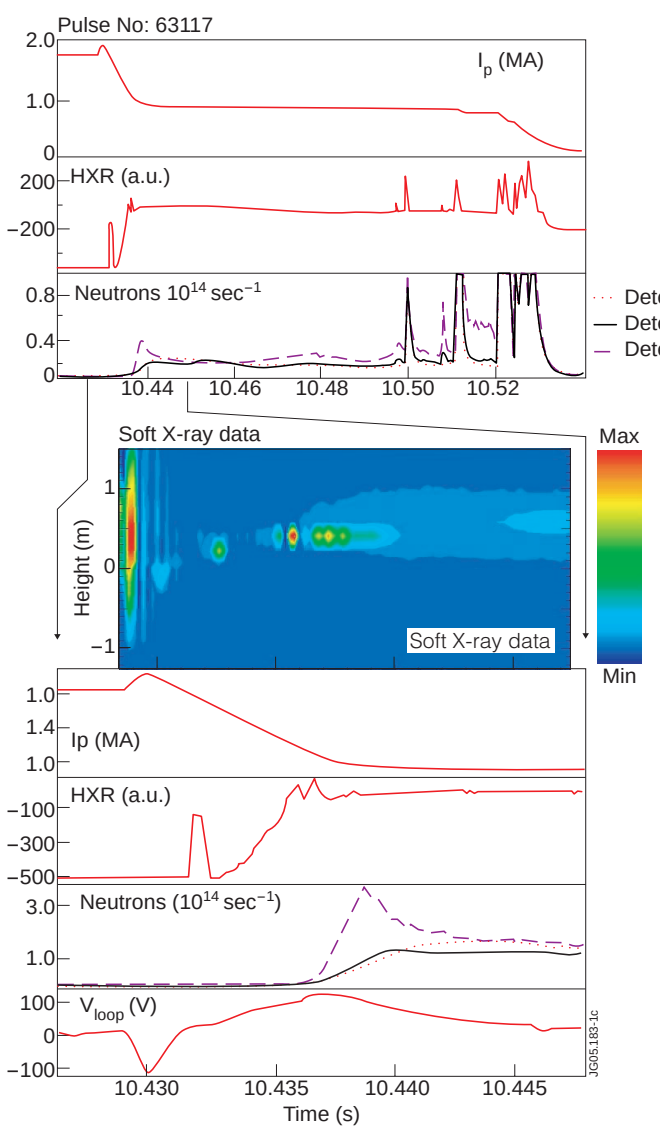

Figure 1: Runaway electrons in Pulse No: 63117 provoked by neon puff. Plasma current (I_p), photo-neutron emission (Neutrons), Hard X-ray (HXR) and loop voltage (V_{loop}) signals are compared to contour plot of the soft X-ray emission measured by horizontal set of detectors. Intensity of the soft X-ray emission is presented in arbitrary units.

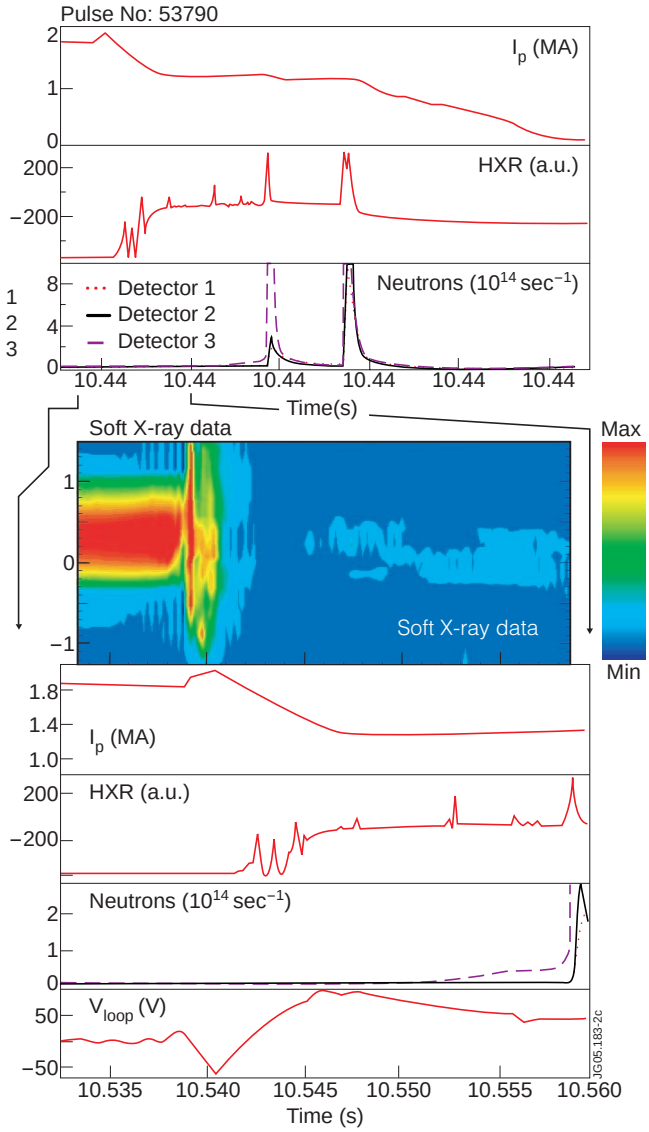

Figure 2: Disruption generated runaway electrons in Pulse No: 53790 (argon puff). Contour plot of the soft X-ray emission measured by horizontal set of detectors is compared to the evolution of plasma current (I_p), photo-neutron emission (Neutrons), Hard X-ray (HXR) and loop voltage (V_{loop}) signals. Intensity of the soft X-ray emission is presented in arbitrary units.

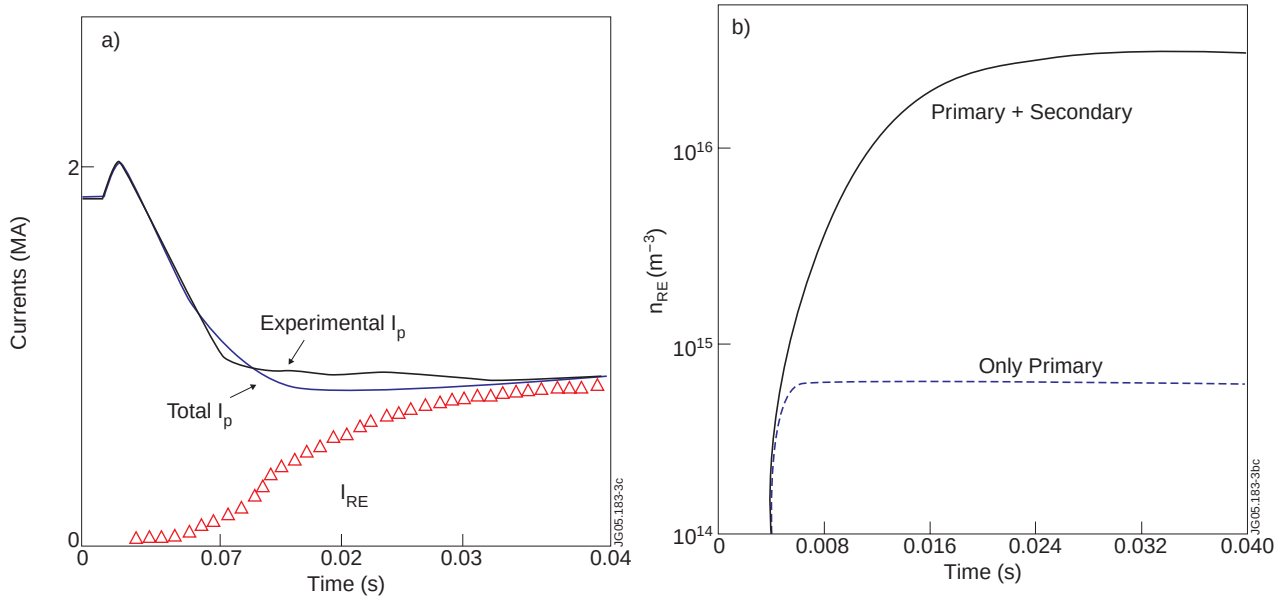

Figure 3: Comparison of the measured plasma current to the calculated total current (RE current+plasma resistive current) at exponential decay of the resistive plasma current with characteristic time 0.01 sec (a). Calculated runaway electron density for primary only and for primary+avalanching mechanisms of runaway electron generation (b).

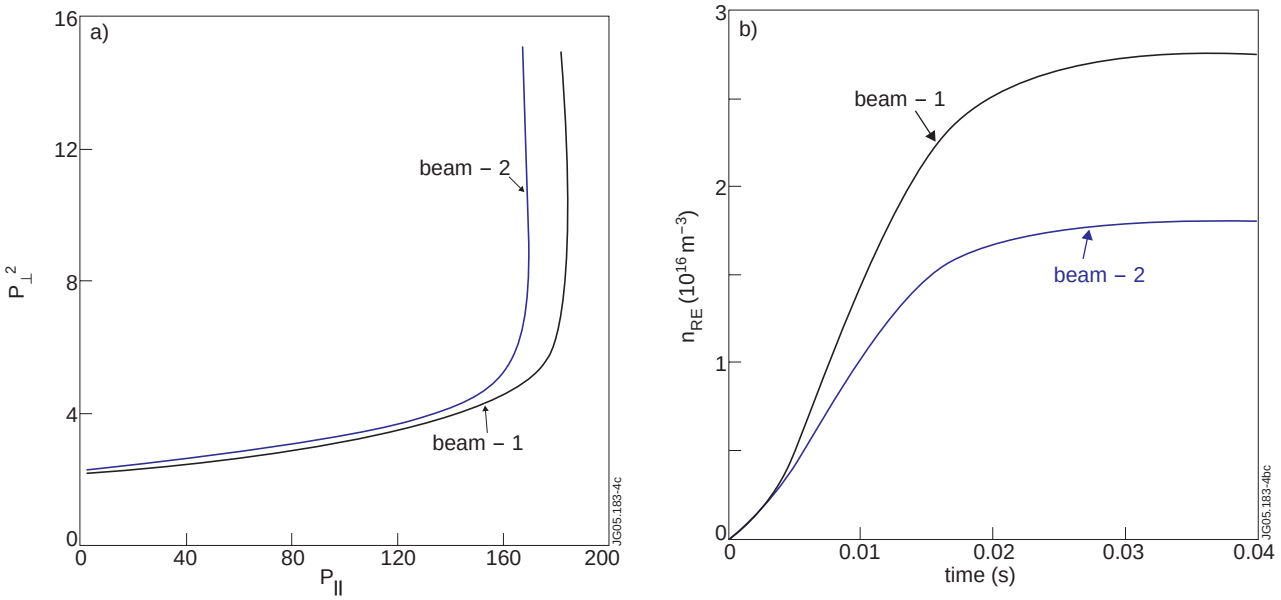

Figure 4: Test electron trajectories in momentum space (a) and evolution of RE densities (b) calculated for two cross-section sizes of RE beams generated during disruptions ($a_{beam2}=2a_{beam1}$). Modelling initial conditions: I_p = 2 MA, T_e = 10 eV $n_e=5\cdot10^{19}$ m^{-3}, Z_{eff} =4, plasma current decay time is 10^{-2} sec.

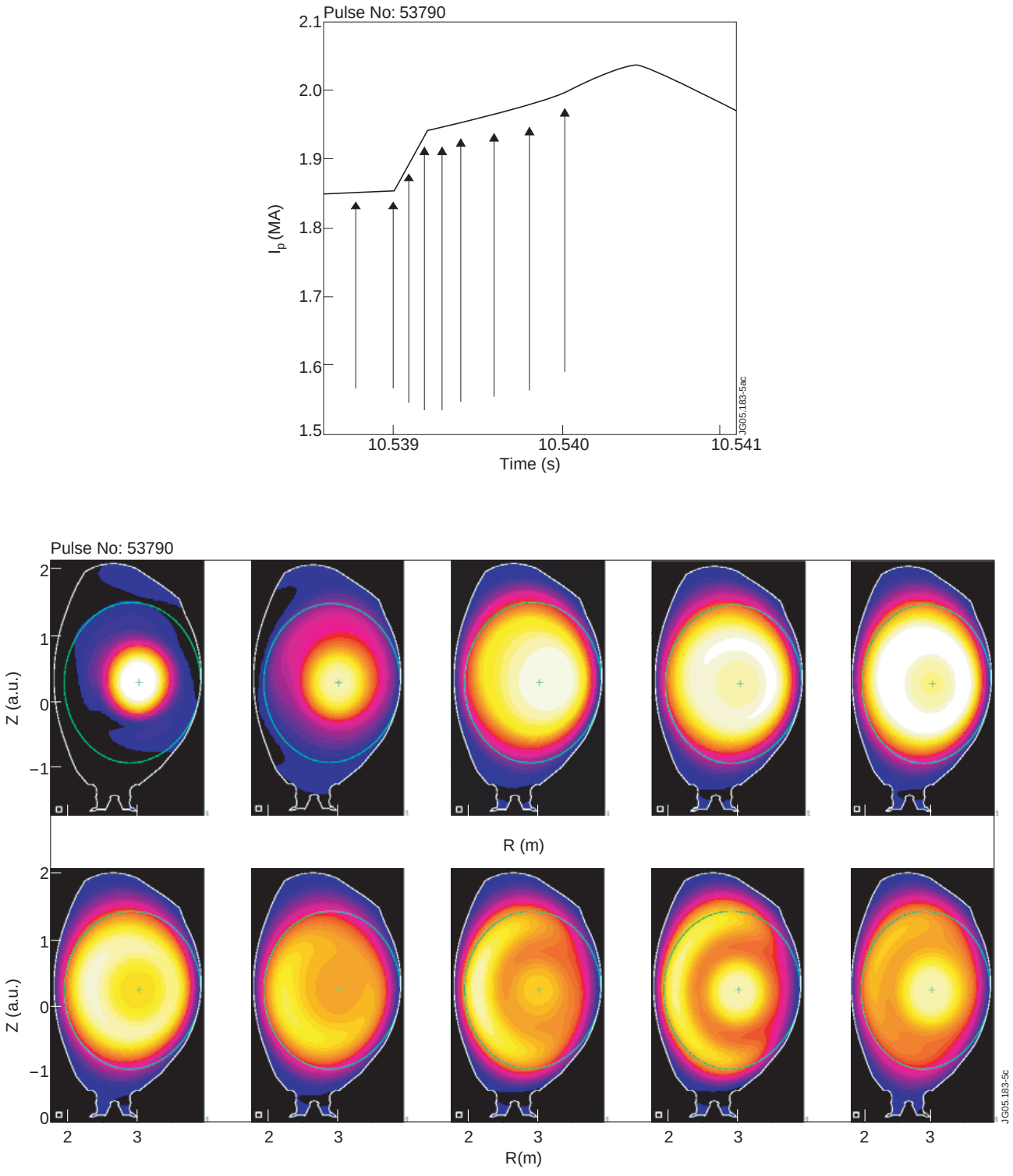

Figure 5: Tomography reconstruction of the soft X ray emission for Pulse No: 53790. Sequence of images is presented for the time points marked by arrows in upper chart, where the plasma current signal during disruption is shown. Reconnection event and abrupt loss of the plasma energy are observed at t=10.5394s. Intensities of soft X-ray emission in all frames are shown in arbitrary units.

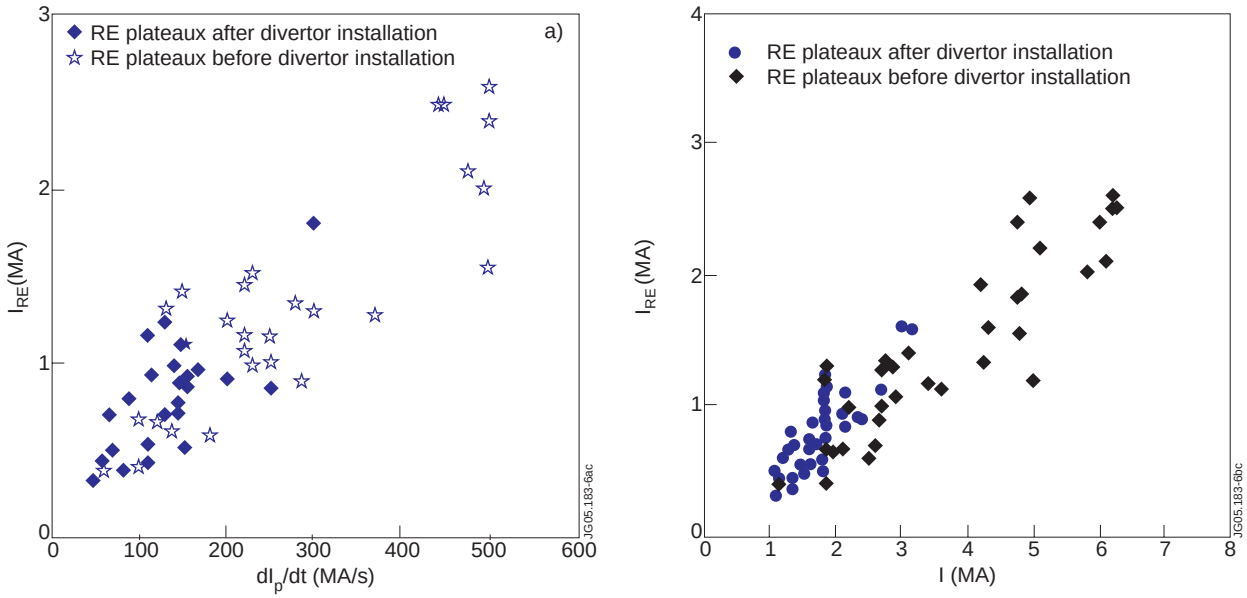

Figure 6: Trends in the creation of RE currents during major disruptions in JET. RE current plateaux vs. the plasma current time derivatives (a) and the pre-disruptive plasma currents (b).

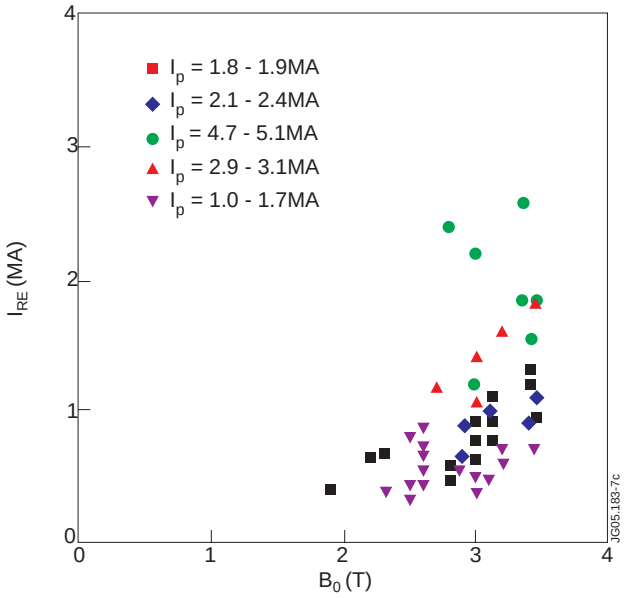

Figure 7: RE plateau values vs. toroidal magnetic fields in JET.